Modeling and evaluation of power transmission of flapping wing nano air vehicle

Alexandre Bontemps, Sébastien Grondel, Thomas Vanneste, Samuel Dupont, Eric Cattan

Modeling and evaluation of power transmission of flapping wing nano air vehicle

Alexandre Bontemps
University of Valenciennes
IEMN, CNRS UMR-8520
Valenciennes, France
alexandre.bontemps@isen.iemn.univ-lille1.fr

Sebastien Grondel
University of Valenciennes
IEMN, CNRS UMR-8520
Valenciennes, France
sebastien.grondel@univ-valenciennes.fr

Thomas Vanneste
University of Valenciennes
IEMN, CNRS UMR-8520
Valenciennes, France
thomas.vanneste@iemn.univ-lille1.fr

Samuel Dupont
University of Valenciennes
IEMN, CNRS UMR-8520
Valenciennes, France
samuel.dupont@univ-valenciennes.fr

Eric Cattan
University of Valenciennes
IEMN, CNRS UMR-8520
Valenciennes, France
eric.cattan@univ-valenciennes.fr

Abstract—In the last decade researchers pursued the development of tiny flying robots inspired by natural flyers. Within this context our main objective is to devise a flying robot-mimicking insect in terms of kinematics and scale using MEMS technologies. For this purpose, an original design has been developed around resonant thorax and wings by the way of an indirect actuation and a concise transmission. Using such a design prototypes with a wingspan of 3 cm and a mass of 22 mg able to lift 75 % of their weights are achieved. As a part of this global goal, this paper presents an innovative power modeling of a flapping-wing nano air vehicle (FWNAV) actuation-transmission system, aiming at a better comprehension of the power transmission from power source to wings, thus allowing future optimization of the actuation efficiency. Considering the multiphysics nature of the prototype a mechatronic approach has been chosen bringing thus a unique model for the whole system. This model has been realized thanks to Bond Graph formalism, which has the crucial advantage to be adapted to multiphysics systems and energetic analysis. After an experimental validation, it is demonstrated that the main parameter conditioning the overall efficiency of the FWNAV is the interaction between coil's current and magnet remanent magnet flux density.

Keywords—Bioinspiration, mechatronic, MEMS, nano air vehicle, Bond Graph, compliant link, electromagnetic actuation

I. INTRODUCTION

Among flying species observed in nature, insects certainly demonstrate the most impressive aerial capacities in terms of hovering, backward flight or sudden acceleration. Moreover, their great robustness allows them to fly after a shock or with damaged wings. Insect diversity therefore brings multiple solutions to generate lift through original design in actuation, structure and wings. For all these reasons, several studies [1–4] as well as observations and experimental data [5–7] on mechanical, kinematical and aerodynamic characteristics of insects, have been carried out. To understand flapping flight and the creation of lift, different strategies have been developed. The one chosen here is based mostly on a heuristic approach to design prototypes with simple wing geometries and a single actuator to generate lift and control the prototype attitude. Very few advanced prototypes with geometric characteristics and masses close to those of an insect exist for more realistic studies [8–12]. This might be due to the fact that traditional robotic mechanisms and macro-scale manufacturing methods can be extremely inefficient on an insect scale due to undesirable surface effects such as adhesion, friction and wear [8]. To overcome this problem, different solutions using MEMS manufacturing processes have been investigated in recent years [9,13,14]. For the construction of an insect-inspired Flapping-Wing Nano Air Vehicle (FWNAV), one priority is to obtain large wing displacements with kinematics similar to those of insects. Another one is to maximize the power-to-weight ratio of the prototype, which requires optimizing the power transmission from the battery to the wings. Therefore, the actuator, as well as the structure, has to be carefully designed to satisfy this compromise. To reach a satisfying structure both priorities have been yet explored. The first one dealing with the design of structure and wings is detailed in a previous paper, demonstrating prototypes able to generate a mean lift force up to 75 % of their weights as measured by an in-house force sensor [13]. The second one presented in this paper is focused on the energetic transmission within the prototype. This study proposes a model of the power transmission in order to evaluate and recognize hypothetical weaknesses. This efficiency analysis is also of great interest in an energetic outlook and especially for autonomy problematic. Moreover, this model of actuation and transmission consists in a first step towards a global model of the prototype. Since, the studied system combines both the mechanical and electromagnetic

fields, a Bond Graph of the system has been set up to obtain a model in a unique formalism. Indeed, this kind of modeling is widely used for multiphysics systems.

The first part of the paper is dedicated to an overview of the prototype and its actuation principle. Second, the global model and its compounds are widely detailed. The different parameters of both mechanical and electromagnetic sub-models are then established thanks to different measurements and analytical studies. Finally, the global model is validated with experimental comparison and the efficiency is determined and discussed.

II. PRINCIPLE

The prototype (figure 1) is primarily composed of a tergum and a pair of wings connected together through compliant links. A central electromagnetic actuator mimicking dorso-ventral muscles of insects is completing the system to initiate and sustain a vibration in the tergum. The transmission of this vibration to the wings needs to be as straightforward as possible, mainly to maximize the system efficiency; therefore, the transmission part is a crucial element of our design. Different solutions have been experimented [15] and the best tradeoff between performance and conception has been found with compliant links [15]. This kind of architecture is realized in SU-8 EPOXY®, which is a photosensitive resin commonly used in MEMS technologies to design micro-mirrors amongst others systems with impressive results [20], [21].Moreover, this material has interesting mechanical properties which are similar to those of insect's wing [16]. Besides the enhanced transmission, the actuation has to be optimized in order to maximize the vibration amplitude of the tergum and thus increase the flapping angle and ultimately the lift generated by the wings.

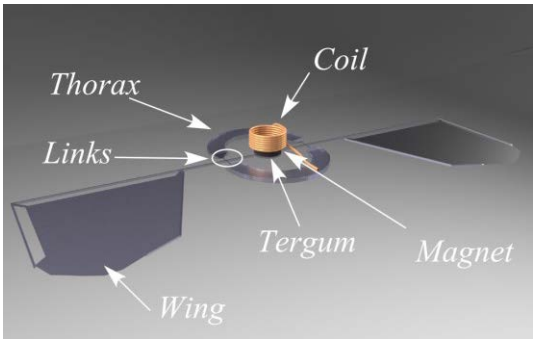

Figure 1: General presentation of the prototype architecture

The electromagnetic actuator is constituted of a magnet stuck to the tergum, which is slipped into a fixed copper coil glued to the thorax, as presented in figure 2. This architecture is easy to manufacture, what is a real advantage at this scale. A cylindrical neodymium-iron-boron magnet (Ni-N48 HKCM®) has been selected, with a thickness of 500 µm and a diameter of 1.5 mm corresponding to a magnet mass of 6.25 mg. The internal magnetic flux provided by the manufacturer is 1.4 T. The coil is made in-house using a 40-µm radius*r*copper covered with a layer of varnish. The coil diameter R is fixed at 2 mm, leaving a 250-µm gap between the coil and the magnet in order to avoid any friction. The electromagnetic force is generated by an interaction between the current travelling the coil and the remanent magnetic field of the magnet that could be expressed by the equation 1.

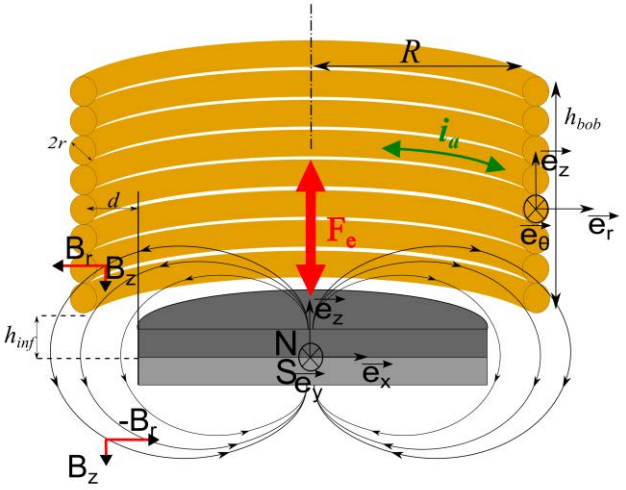

Figure 2: Diagram of the electromagnetic actuator with the different parameters and a view of the field lines

$$\boldsymbol{F_e} = i_a \cdot \boldsymbol{dl} \wedge \boldsymbol{B} \quad (1)$$

where i_a is the current inside the coil flowing along e_θ, and $\boldsymbol{B}$ the magnetic flux density passing through the coil. Only the vertical component of the force is here constructive, indeed the magnet and the coil are supposed to be perfectly concentric and cylindrical. In this case, the integral of the radial component of the force on the coil is null, and the vertical component of the force is generated exclusively by the interaction between B_r (the radial component of the magnetic flux density) and i_a.

III. MODELING

As a first step towards a complete prototype model, this paper presents the actuator and transmission parts of the model, composed of two blocks (figure 3 (a)). First an electromagnetic system, shown on the figure 4, composed of the coil and the magnet modeling the transformation of the electric power P_a (U_a, i_a) into a mechanical power P_m $(F_e, \dot{z})$ through interaction of both electric fields generated in the coil and remanent magnetic fields of the magnet. Second, a mechanical resonator, shown in the figure 5, constituted of the magnet, the tergum and the links. The mechanical resonator will dissipate or store power under different ways resulting in a mechanical power P_u $(F_u, \dot{z})$ transmitted to the wings.

The system studied here is composed by the ensemble coil, magnet, tergum and links (figure 3 (b)). Although, this modeled system highlighted in the red frame in the figure 3 (a) does not take into account the wings or the battery, the battery is still present via a source S_f of an electrical flux i_a. The main goal of this analysis is to compare the input power P_a injected in the coil with the mechanical one available to move the wings. For this purpose, the two blocks, i.e. the electromagnetic system and the mechanical resonator, are

firstly studying separately before being coupled to form the global model.

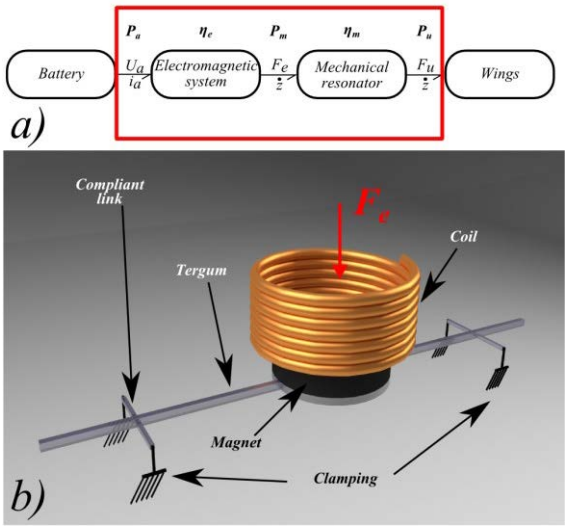

Figure 3: (a) Bond Graph representation of the whole system, the red frame corresponding to the modeled system. (b) Schematic view of the modeled-system composed of coil, magnet, tergum and links

A. Bond Graph model

In one hand, the electromagnetic part is modeled with three elements as it is presented in the figure 4 through an electrical equivalent circuit and a Bond Graph model: a R-element representing the coil resistor (R_b), and a variable gyrator (MGY) with a parameter $k_{em}(z)$ symbolizing the transformation of electrical power into mechanical one [17]. This last element expresses the relation between the current in the coil i_a and the mechanical force generated F_e. The radial compounds of the magnetic flux density crossing each whorl of the coil is considered as equal to the mean radial compounds of the magnetic flux density crossing the whole coil $B_m(z)$, which still depends of the magnet vertical position z. R and n represent the coil diameter and its whorl number, respectively. To connect these both elements a 1-junction is used to indicate that the current generator, the resistor and the gyrator are serially connected.

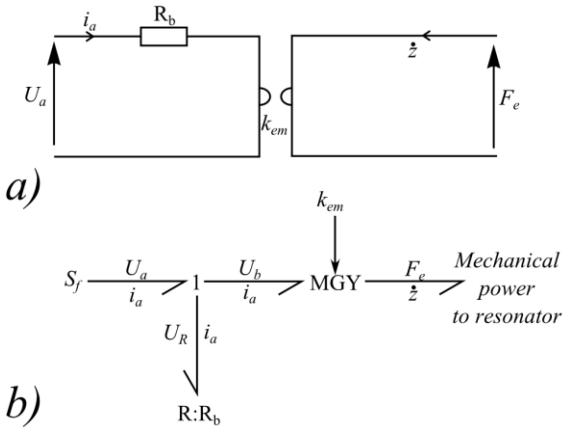

Figure 4: (a) Representation of the electromagnetic system (a) through an electrical equivalent circuit, (b) through Bond Graph formalism

These relationships are expressed by these two equations:

$$\begin{cases} U_R = R_b \cdot i_a \\ F_e = B_m(z) \cdot 2 \cdot \pi \cdot R \cdot n \cdot i_a = k_{em}(z) \cdot i_a \end{cases} \quad (1)$$

In the other hand, the mechanical system composed of the magnet, the tergum and the links (MTL-system) is identified as a spring-mass system (figure 5 (a)). This resonator could be characterized by a C-element for its stiffness ($1/k_{eq}$), a I-element for its mass (m_{eq}) and a R-element for its damping (R_{eq}) as represented on the figure 5 (b). Finally, a 1-junction is used to express the Newton's second law (equation 2):

$$m_{eq}\ddot{z} + R_{eq}\dot{z} + k_{eq}z = F_e(t) \quad (2)$$

In order to characterize all parameters (R_b, R_{eq}, m_{eq} k_{eq} and $k_{em}(z)$) of the both blocks different tools and method have been used and are presented in section B.

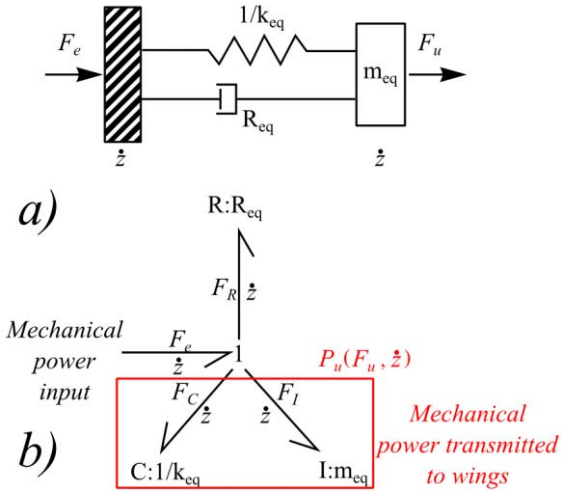

Figure 5: (a) Representation of the mechanical resonator (a) through a spring-mass representation, (b) through Bond Graph formalism

B. Parameter estimation

1) Electromagnetic system

To obtain the coil resistance R_b analytical calculi has been compared to experimental measurements; results obtained are summarized in the table 1. It has to be duly noted that the coil is only represented by a resistor as a more complete study realized in [15] proved that its inductive behavior can be neglected mainly due to the low frequency of the current i_a.

Table 1: Comparison of 8-whorls coil resistance different wire diameters

Wire diameter [µm]	Resistance value [mΩ]	
	Theoretical values	*Measured values*
25	435	[425-577]
40	170	[175-182]
60	75	[65-93]

The electromagnetic coupling coefficient $k_{em}(z)$ depends of the coil radius R, the whorl number n and the mean radial compounds of the magnetic flux density crossing the whole coil $B_m(z)$. A finite elements simulation [13] has been used to

establish this last parameter. For this purpose, B_m *(z)* has been evaluated along z-axis at a radial distance *d* of 250 µm from the magnet. This value represents the technological minimum that could be reached considering the handmade assembly [13]. Then an 8-whorls coil made of a 60-µm radius wire is considered and the sliding average of the mean radial magnetic flux density, $B_m(z)$ is calculated on the bobine height (h_{bob}, figure 2). The determination of these parameters allows evaluating the electromagnetic actuator system.

2) Mechanical resonator

First, the equivalent mass m_{eq} of the system is determined through experimental method. Thus the different component of the MTL-system are weighted on a high-precision scale (Mettler Toledo XP-26), able to measure 1 µg. 13 samples have been weighted and the equivalent masses obtained are between 5.97 and 6.85 mg. This mass mostly corresponds to the magnet that is around 6 mg. Second, a modal analysis has been run in order to determine the first resonant frequency of the MTL-system. Indeed, considering the equation 3, the knowledge of m_{eq} and f_1 enables to figure out the equivalent stiffness of the system, k_{eq}.

$$f_1 = \frac{1}{2\pi}\sqrt{\frac{k_{eq}}{m_{eq}}} \tag{3}$$

To realize this modal analysis, a finite element simulation has been set up with each link clamped at its thorax side, as presented on the figure 6. Moreover, a parametric analysis has been developed by changing, in one hand the beam thickness, which plays a major role in beam stiffness according to equation 4, and in the other hand the SU-8 Young's modulus. Indeed, thanks to different studies it is known that this modulus could vary roughly between 3.5 to 5.5 GPa.

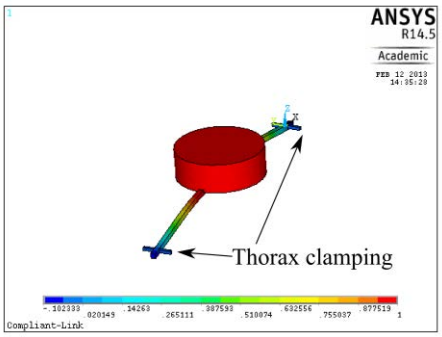

Figure 6: Modal analysis through the finite element method figuring the MTL-system

$$k_{beam} = E_{SU-8} \cdot w_{beam} \cdot \frac{t_{beam}^3}{L_{beam}^3} \tag{4}$$

Thanks to these simulations and considering m_{eq} variations, the equivalent stiffness lies between 17 N.m^{-1} and 37.8 N.m^{-1}. In order to confirm these simulation results, an experimental bench composed of a Femtotools® force sensor and a micrometric displacement pad has been set up (figure 7). The force sensor is fixed to the pad and displaced by 10-µm steps; at each step, while the reaction force exerted by the MTL-system on the sensor is measured. Considering Hooke's law (equation 5), the knowledge of F_r allows to determine experimentally the equivalent stiffness k_{eq} of the system.

$$F_r = k_{eq} \cdot \Delta z \tag{5}$$

For a global displacement of 90 µm in both directions, data interpolation exhibits an equivalent stiffness of 18.7 N.m^{-1} in one direction and 19.6 N.m^{-1} in the other direction. Hence, these experimental results confirm the analytical value previously obtained with finite element analysis.

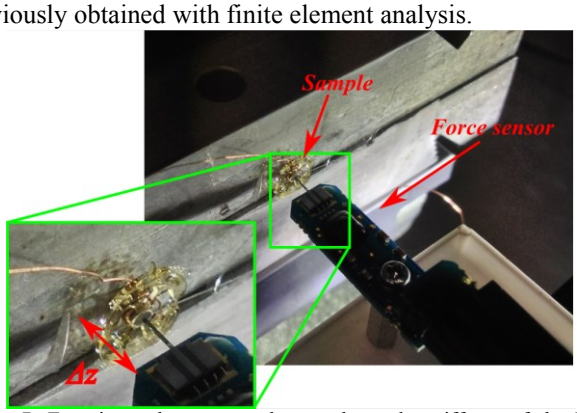

Figure 7: Experimental set-up used to evaluate the stiffness of the MTL-system

The last parameter, which needs to be evaluated, is the equivalent damping R_{eq}. This parameter overlays numerous damping mechanisms (thermoelastic, viscoelastic, aerodynamic, clamping, etc.) that are very difficult to evaluate analytically. Consequently, another test bench has been set up in order to experimentally evaluating this parameter. First, the MTL-system is excited to its first resonant frequency f_1. Second, when the resonator has reached a stable state, the excitation is stopped and the transient deceleration of the resonator is monitoring thanks to a Keyence LK G-32 displacement sensor. The envelop curves could be expressed as an exponential decrease

$$\alpha(t) = A.e^{-\xi.2\pi f_1 t} \tag{6}$$

where ξ could be determined with the equivalent parameters R_{eq}, k_{eq} and m_{eq}:

$$\xi = \frac{R_{eq}}{2 \cdot \sqrt{k_{eq} m_{eq}}} \tag{7}$$

With the mean values of k_{eq} and m_{eq} previously determined, 19.1 N.m^{-1}, 6.29 mg respectively, the equivalent damping obtained is between 0.00045 and 0.001. These results are also summarized in the table 2 for clarity sake.

Table 2: Recap of the theoretical, measured and used values in the Bond Graph model for the mechanical parameters

	Theoretical values	***Measured values***	***Used value***
k_{eq}[N.m^{-1}]	[17;37.8]	[18.7;19.6]	19.1
m_{eq} [mg]	[6.16;7.04]	[5.97;6.85]	6.78
R_{eq}		[0.00045;0.001]	0.00085

To form the complete Bond Graph model of our prototype, each sub-model, the electromagnetic system of the figure 4 (b) and the mechanical resonator of the figure 5 (b), just has to be coupled together, here via a serial connection.

IV. SIMULATION & EXPERIMENTAL VALIDATION

Even if the complete Bond Graph model up and running, its validation, among other things, with experimental data is primordial to evaluate the soundness of the above determined parameters before rushing in further investigations such as the power efficiency.

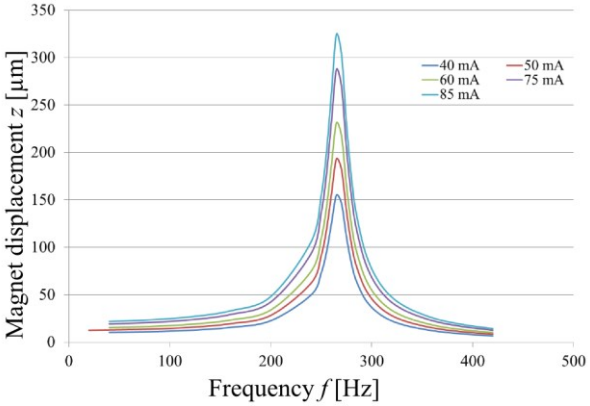

Figure 8: MTL-system mechanical response symbolized by the displacement of the magnet z for different sinusoidal excitations of amplitude i_a and a frequency f.

To check the model ability, the resonator response is simulated for sinusoidal current input of different values (i_a) and frequencies (f). The magnet displacement z obtained with the simulation exhibits the typical response of a mechanical resonator. It should be noted that the resonant frequency of 267 Hz is independent of the displacement amplitude (figure 8) highlighting the absence of any non-linearity in the system.

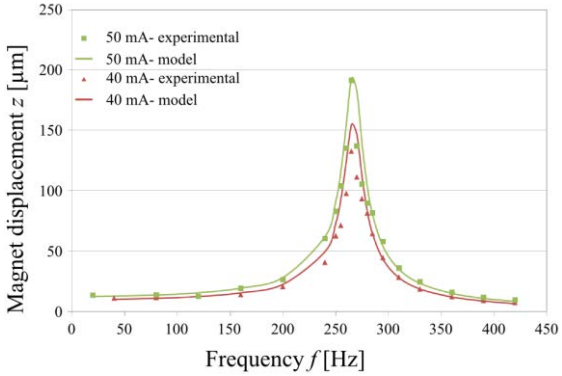

Figure 9: Comparison of MTL-system response in simulation (lines) and in experimental (dots) results for small magnet displacement (less than 200 µm)

To measure experimentally and compare magnet displacement with simulations results an experimental bench has been set up. The thorax of the prototype is fixed and the actuator is powered by an external source while the fundamental resonant frequency of the wings is manually adjusted and the magnet displacement tracked. In order to preserve the same load between the simulation and the experimentation, the wings of the prototype are cut as near as possible from the links. As presented on the figure 9, first tests highlight a very good correlation between experimental results and simulations. Nevertheless, for large magnet displacement, an increase of the resonant frequency due to geometric non-linearities is appearing. The Duffing equation [18] proposes to model these non-linearities by the addition of a non-linear stiffness k_{nl}. In this case the equation 2 becomes:

$$m_{eq}\ddot{z} + R_{eq}\dot{z} + k_{eq}z + k_{nl}z^3 = F_e(t) \quad (8)$$

Through a heuristic approach, a value of $126 \cdot 10^6$ N.m^{-3} has been chosen for k_{nl}. As demonstrated on the figure 10, a satisfying correlation in frequency shift as well as in the response amplitude is observed which validates the complete Bond Graph model.

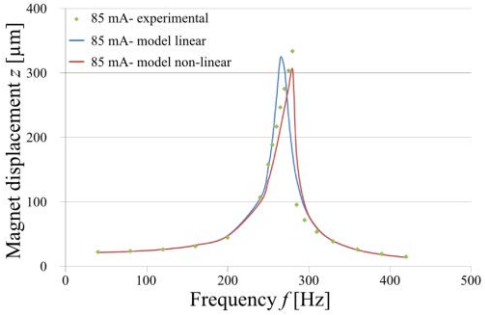

Figure 10: Comparison of MTL-system response between experimental results (green dots), linear simulation (blue line) and non-linear simulation (red line)

V. EFFICIENCY EVALUATION

In order to evaluate the actuator efficiency, the power available for the wings corresponding to the one stored under kinematics P_I (F_I, $\dot{z}$) and potential energy P_C (F_C, $\dot{z}$) in the mechanical resonator need to be evaluated. Considering the results obtained above, the complete Bond Graph model has been used to evaluate the efficiency of the MTL-system.

Its efficiency η_t can be defined as the ratio between the input power P_a and the power transmitted to the wings P_u. In our case, i.e. without wing model, this power corresponds to the sum of P_I (F_I, $\dot{z}$) and P_C (F_C, $\dot{z}$).

$$\frac{P_u}{P_a} = \eta_t = \eta_e \cdot \eta_m \quad (9)$$

It could also been expressed as the product of the electromagnetic sub-model efficiency η_e and mechanical sub-model η_m. This indicator is evaluated with the Bond Graph model presented in precedent sections with 20-SIM® software. The results obtained exhibit an overall efficiency of 1.4 %. Indeed, for an electrical input power P_a of 288 µW, corresponding to a current (rms) of 60 mA and a voltage (rms) of 4.8 mV, the mechanical output power available to actuate wings P_u is 4.6 µW. To refine this analysis, η_e, η_m are examined separately.

In one hand, the figure 11(a) brings to light that the power dissipated through Joule effect in the coil represents 98 % of whole losses. In the other hand, mechanical damping in the resonator dissipates only 27 % of the whole losses as it could be seen in the figure 11(b). This analysis leads to the conclusion that main energetics losses come from electromagnetic actuator and more precisely from the coil. In order to increase the actuator efficiency two ways might be followed, first reduce the current into the coil and second decrease the coil resistance. The counterpart of such measure is that the radial compound of the magnetic flux density needs

to be increased at the coil neighborhood to maintain the electromagnetic force generated F_e.

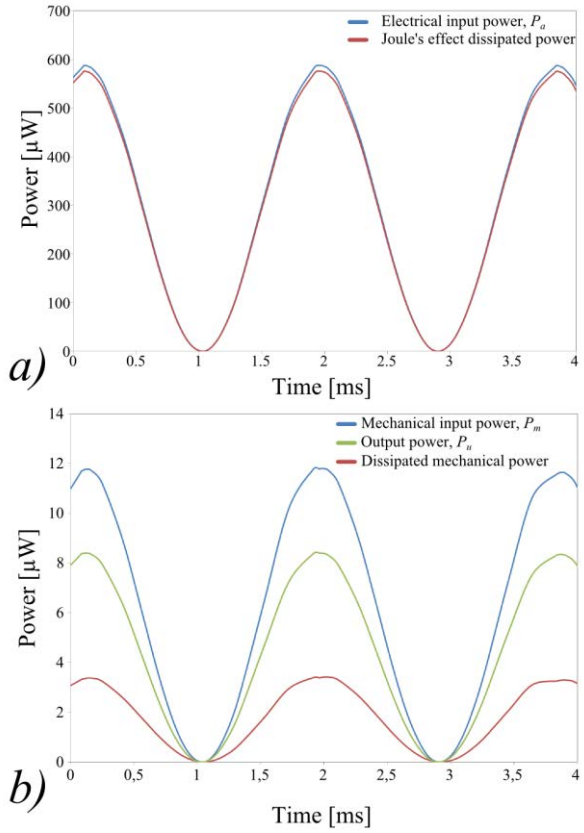

Figure 11: Presentation of simulation results: (a) Efficiency characterization of electromagnetic sub-model, input power (blue line) and power dissipated through Joule effect (red line). (b) Efficiency of mechanical sub-model, input power (blue line), power dissipated (red line) and output mechanical power (green line)

VI. CONCLUSION & PERSPECTIVES

This paper proposes a Bond Graph model of a FWNAV actuator composed of a linear electromagnetic actuator and a mechanical resonator which has been experimentally validated and used to evaluate actuator's efficiency. This energetic evaluation indicates that the electromagnetic actuator and more precisely the interaction between coils current and magnet remanent magnet flux density needs to be improved. The main way to improve this interaction is in the coil, indeed different material might replace the cupper, its position could also been optimized. A more complete model integrating wings will be available in the near future allowing a global evaluation of a FWNAV efficiency.

ACKNOWLEDGMENT

This research was financially supported by the Agence Nationale de la Recherche (ANR-09-BLAN-0110), and the Fondation d'Entreprise EADS.

REFERENCES

[1] Ennos A R 1987 A comparative study of the flight mechanism of Diptera *J. Exp. Biol.* **127** 355

[2] Combes S., Daniel L T 2003 Flexural stiffness in insect wings I. Scaling and the influence of wing venation *J. Exp. Biol.* **206** 2979–87

[3] Dickinson M H 1999 Wing Rotation and the Aerodynamic Basis of Insect Flight *Science (80-.).* **284** 1954–60

[4] Ellington C P 1984 The Aerodynamics of Hovering Insect Flight. I. The Quasi-Steady Analysis *Philos. Trans. R. Soc. B Biol. Sci.* **305** 1–15

[5] Dudley R and Ellington C P 1990 Mechanics of forward flight in bumblebees: II. Quasi-steady lift and power requirements *J. Exp. Biol.* **148** 53

[6] Dickinson M H and Götz K G 1996 The wake dynamics and flight forces of the fruit fly Drosophila melanogaster *J. Exp. Biol.* **199** 2085–104

[7] Fry S N, Sayaman R and Dickinson M H 2005 The aerodynamics of hovering flight in Drosophila. *J. Exp. Biol.* **208** 2303–18

[8] Wood R J, Avadhanula S, Sahai R, Steltz E and Fearing R S 2008 Microrobot Design Using Fiber Reinforced Composites *J. Mech. Des.* **130** 052304

[9] Dargent T, Bao X Q, Grondel S, Brun G Le, Paquet J B, Soyer C and Cattan E 2009 Micromachining of an SU-8 flapping-wing flying micro-electro-mechanical system *J. Micromechanics Microengineering* **19** 085028

[10] Groen M, Bruggeman B and Remes B 2010 Improving flight performance of the flapping wing MAV DelFly II *International Micro Air Vehicle conference and competitions (IMAV 2010)* (Braunschweig, Germany)

[11] Park J and Yoon K 2007 Development of bio-mimetic composite wing structures and experimental study on flapping characteristics *Robot. Biomimetics* 25–30

[12] Pornsin-Sirirak T N, Lee S, Nassef H, Grasmeyer J, Tai Y, Ho C and Keennon M 2000 MEMS wing technology for a battery-powered ornithopter *Micro Electro Mech. Syst. 2000.* **043** 799–804

[13] Bontemps A, Vanneste T, Paquet J-B, Dietsch T, Grondel S and Cattan E 2013 Design and performance of an insect-inspired nano air vehicle *Smart Mater. Struct.* **22** 014008

[14] Pornsin-Sirirak T N T, Tai Y Y C, Nassef H and Ho C M 2001 Titanium-alloy MEMS wing technology for a micro aerial vehicle application *Sensors Actuators A Phys.* **89** 95–103

[15] Bontemps A 2013 *PhD thesis, Prototypage d'un Objet Volant Mimant l'Insecte* (University of Valenciennes)

[16] Bao X Q, Bontemps A, Grondel S and Cattan E 2011 Design and fabrication of insect-inspired composite wings for MAV application using MEMS technology *J. Micromechanics Microengineering* **21** 125020

[17] Karnopp D 1985 Bond graph models for electromagnetic actuators *J. Franklin Inst.*

[18] Duffing G 1918 Erzwungene Schwingungen bei veranderlicher eigenfrequenz *Vieweg, Braunschweig*